New concept for the ground-state band in ^{20}Ne within a microscopic cluster model

Bo Zhou,[1,2,*] Zhongzhou Ren,[1,3,†] Chang Xu,[1,‡] Y. Funaki,[4] T. Yamada,[5] A. Tohsaki,[2] H. Horiuchi,[2,6] P. Schuck,[7,8] and G. Röpke[9]

[1]*Department of Physics, Nanjing University, Nanjing 210093, China*
[2]*Research Center for Nuclear Physics, Osaka University, Osaka 567-0047, Japan*
[3]*Center of Theoretical Nuclear Physics, National Laboratory of Heavy-Ion Accelerator, Lanzhou 730000, China*
[4]*Nishina Center for Accelerator-Based Science, The Institute of Physical and Chemical Research (RIKEN), Wako 351-0198, Japan*
[5]*Laboratory of Physics, Kanto Gakuin University, Yokohama 236-8501, Japan*
[6]*International Institute for Advanced Studies, Kizugawa 619-0225, Japan*
[7]*Institut de Physique Nucléaire, CNRS, UMR 8608, F-91406 Orsay, France*
[8]*LPMMC, UMR 5493, F-38042 Grenoble 9, France*
[9]*Institut für Physik, Universität Rostock, D-18051 Rostock, Germany*

(Received 30 March 2012; revised manuscript received 24 May 2012; published 3 July 2012)

We propose a generalized wave function based on the flexible original THSR (Tohsaki, Horiuchi, Schuck, Röpke) wave function [A. Tohsaki *et al.*, Phys. Rev. Lett. **87**, 192501 (2001)], which is applicable to studies of general cluster structures in nuclei. The ground-state band in ^{20}Ne is investigated by using this generalized wave function and the energies obtained agree well with the experimental values. Moreover, it is found that the single generalized THSR wave functions almost completely coincide with the exact solutions of the $\alpha+^{16}$O resonating group method for the ground-state band in ^{20}Ne. For the ground state, for instance, the squared overlap between them is 99.3%. This indicates that the THSR model can also be extended to study more compact cluster states in nuclei such as, e.g., the ground-state band in ^{20}Ne.

DOI: 10.1103/PhysRevC.86.014301 PACS number(s): 21.60.Gx, 27.30.+t

I. INTRODUCTION

Clustering, one of the most interesting features of nuclei, is a very important aspect of many-body systems [1,2]. In light nuclei, clustering as well as single-particle motion plays a significant role in understanding the structures of nuclei [3,4]. A very novel cluster state in light nuclei, α condensation, has attracted increasing interest in recent years [5–13]. This α-condensation state can be considered as the one where the center-of-mass motion of each α cluster in nuclei occupies the same 0S orbit. The proposed THSR wave function is very suitable for describing this dilute gas-like state, which indeed leads us to have a new perspective for the $n\alpha$ structure in light $4n$ nuclei (see Refs. [14] and [15] and references therein). In this microscopic framework, the gas-like states of α particles in ^{12}C [16] and ^{16}O [17,18] near the threshold energies have been identified as the most possible candidates for the α-condensation states. Very recently, a new scattering experiment provided evidence for the existence of the excited rotational state 2_2^+ built on the Hoyle state in ^{12}C [19]. The 2_2^+ state of ^{12}C can be described in the THSR model [9], which is a good candidate for an excited α-condensate state. As for the nucleus ^{8}Be, the single 0^+ THSR wave function agrees almost completely with the solution superposing 30 Brink type 0^+ wave functions [20]. Therefore, the THSR wave function gives a new picture for ^{8}Be, namely, a very dilute gas-like state structure of two α particles rather than a dumbbell structure [6].

The THSR wave function is characterized by a spatial extension in which clusters make delocalized motions, which is quite successful in describing the dilute gas-like states in light nuclei. Besides, considering that the THSR wave function contains two limiting configurations [5], namely, the shell model and the pure α gas structure, it is natural to extend this idea to more general non-gas-like cluster structures in nuclei. In fact, the more shell-model-like ground states of ^{12}C and ^{16}O have also been described in the framework of the THSR wave function [5], which supports this extension. Thus, we propose a generalized THSR wave function for studying general cluster structures in nuclei which are more compact. This is expected to provide a new picture for understanding cluster structures in nuclei.

The intrinsic structure of the ground-state band in ^{20}Ne has a transient character, in which the shell model and the $\alpha+^{16}$O structure both play an important role [22–26]. In the early stage, the *sd*-shell model [27,28], which treated the ^{16}O as an inert core reproduced the level structure of the ground-state band in ^{20}Ne. However, it was found that some correlations were not included in this model. Next, the α correlations were taken into account, and one of the authors and Ikeda [29] proposed that the ground-state band and $K^\pi = 0^-$ band could be considered as an inversion doublet heteropolar $\alpha+^{16}$O configuration. They stated further that the ground-state band had a transient character from the shell-model-like structure to the $\alpha+^{16}$O structure, which was different from the well-developed dinucleus structure in the $K^\pi = 0^-$ band. This important conclusion has been confirmed by subsequent cluster models, such as the resonating

*zhoubo@rcnp.osaka-u.ac.jp
†zren@nju.edu.cn
‡cxu@nju.edu.cn

group method (RGM) [30] and the Brink cluster model [31]. It is noted that the relative distance between the α cluster and the ^{16}O cluster is adopted as a variational parameter in these models, which provides a rigid compact picture in the $\alpha+^{16}$O model space for understanding the ground-state band in ^{20}Ne. Later, in the framework of antisymmetrized molecular dynamics (AMD) without assuming the existence of clusters, the calculated results show that the $\alpha+^{16}$O configuration constitutes a predominant configuration in the ground-state band and the more cluster-model-like state changes to the more shell-model-like state as the spin goes up [32]. Thus, both the shell model picture and the cluster picture are indispensable for understanding the ground-state band in ^{20}Ne. In order to treat the nuclear states in such transient situation in ^{20}Ne, the adopted model should include both limits, that is, the shell model states at one end of the microscopic treatment and the molecular states at the other extreme [22].

The purpose of this work is to study the ground-state band in ^{20}Ne using a generalized THSR wave function. At first, we introduce this generalized THSR wave function, as a natural extension of the original THSR wave function. Then the energy surfaces corresponding to different spin-projected states in ^{20}Ne are discussed. In order to clarify this wave function further, we make a comparison between our generalized THSR model and the Brink cluster model.

The paper is organized as follows. In Sec. II, we introduce our generalized THSR model. The results and our discussion are given in Sec. III. We provide a summary in Sec. IV.

II. THE MODEL

A. Generalized THSR wave function for ^{20}Ne

The deformed $n\alpha$ condensed wave function [6] has been proposed by one of the authors as a natural extension of the spherical THSR wave function, which can be expressed by a superposition of Brink's $n\alpha$ cluster wave functions,

$$\Phi_{n\alpha}(\beta_x,\beta_y,\beta_z) = \int d^3R_1\ldots d^3R_n \exp\left\{-\sum_{i=1}^{n}\left(\frac{R_{ix}^2}{\beta_x^2}+\frac{R_{iy}^2}{\beta_y^2}+\frac{R_{iz}^2}{\beta_z^2}\right)\right\} \times\Phi^B(\boldsymbol{R}_1,\ldots,\boldsymbol{R}_n) \quad (1)$$

$$\propto \mathscr{A}\left[\prod_{i=1}^{n}\exp\left\{-\left(\frac{2X_{ix}^2}{B_x^2}+\frac{2X_{iy}^2}{B_y^2}+\frac{2X_{iz}^2}{B_z^2}\right)\right\}\phi(\alpha_i)\right], \quad (2)$$

where $B_k^2=b^2+2\beta_k^2$ $(k=x,y,z)$, and $\boldsymbol{X}_i$ is the center-of-mass coordinate of the ith α cluster α_i. $\Phi^B(\boldsymbol{R}_1,\ldots,\boldsymbol{R}_n)$ is the Brink wave function, in which the relative motion of 0S α particles can be represented by the generator coordinate $\boldsymbol{R}_i$. $\phi(\alpha_i)$ is the intrinsic wave function of an α particle. The center-of-mass motion of each of the $n\alpha$ particles occupies the same deformed orbit, $\exp(-2X_{ix}^2/B_x^2-2X_{iy}^2/B_y^2-2X_{iz}^2/B_z^2)$. From this point of view, this wave function is very convenient for the description of the $n\alpha$ gas-like structures in light nuclei. In order to study more general cluster structures of nuclei in the framework of the THSR model, we make a quite straightforward extension of the deformed THSR wave function,

$$\Phi_{\text{cluster}}(\beta_x,\beta_y,\beta_z) = \int d^3R_1\ldots d^3R_n \exp\left\{-\sum_{i=1}^{n}\left(\frac{R_{ix}^2}{\beta_{ix}^2}+\frac{R_{iy}^2}{\beta_{iy}^2}+\frac{R_{iz}^2}{\beta_{iz}^2}\right)\right\} \times\Psi^B_{\text{cluster}}(\boldsymbol{R}_1,\ldots,\boldsymbol{R}_n) \quad (3)$$

$$\propto \mathscr{A}\left[\prod_{i=1}^{n}\exp\left\{-A_i\left(\frac{X_{ix}^2}{B_{ix}^2}+\frac{X_{iy}^2}{B_{iy}^2}+\frac{X_{iz}^2}{B_{iz}^2}\right)\right\}\phi(C_i)\right], \quad (4)$$

where

$$B_{ik}^2=2b_i^2+A_i\beta_{ik}^2 \quad (k=x,y,z). \quad (5)$$

In the above equations, $\boldsymbol{X}_i$ is the center-of-mass coordinate of cluster C_i. Different clusters C_i have different variational parameters β_i, b_i and different mass numbers A_i. $\Psi^B_{\text{cluster}}(\boldsymbol{R}_1,\ldots,\boldsymbol{R}_n)$ is nothing but the general Brink cluster model wave function [33].

It should be noted that there also appear two limits in the generalized THSR wave function. When $\beta\to 0$ as a limit, the normalized wave function Eq. (4) coincides with the shell-model Slater determinant. When $\beta\to\infty$ as the other limit, this wave function corresponds to a state of n free clusters. In addition, in terms of the mathematical form of the generalized THSR wave function, the cluster subunit is no longer limited to an α particle. For example, the $d+\alpha$ cluster structure for ^{6}Li can also be treated in the generalized THSR model.

In fact, Eq. (3) can be seen as a particular case of the generator coordinate method (GCM). The weight function is adopted as a restricted Gaussian function. After integration of the generator coordinates, namely, Eq. (4), the physics meaning of Eq. (3) can be easily understood.

It is interesting to compare this generalized THSR wave function with the Brink cluster model wave function. The most important difference between the two wave functions is that the generalized THSR function is delocalized [20], in which the center-of-mass motions of clusters are determined by the parameter β, while the Brink model is localized and the motions of different clusters are represented by the different generator coordinates $\boldsymbol{R}_i$. Thus, the Brink cluster model tends to treat rigid cluster structures of nuclei, while the generalized THSR wave function is very suitable for describing loosely bound or not geometrical cluster structures. The famous Hoyle state of ^{12}C is a typical example of the latter. The Brink cluster model fails to describe this state, while the THSR model works very well [16]. However, if a system displays a linear chain structure or other rigid structures, the generalized THSR wave function may not be suitable for describing the system. This is because the clusters in the nucleus cannot be rearranged in some geometric fashion restricted by the parameter β.

As the first case, we perform a detailed study of the ground-state band in ^{20}Ne within this microscopic cluster model. The generalized THSR wave function for ^{20}Ne can be

written as

$$\Phi_{\rm Ne}(\beta_x,\beta_y,\beta_z) = \int d^3R_1 d^3R_2 \exp\left\{-\left(\frac{R_{1x}^2}{\beta_{1x}^2}+\frac{R_{1y}^2}{\beta_{1y}^2}+\frac{R_{1z}^2}{\beta_{1z}^2}\right)\right\} \times \exp\left\{-\left(\frac{R_{2x}^2}{\beta_{2x}^2}+\frac{R_{2y}^2}{\beta_{2y}^2}+\frac{R_{2z}^2}{\beta_{2z}^2}\right)\right\} \times \Phi_{\rm Ne}^B(\boldsymbol{R}_1,\boldsymbol{R}_2), \tag{6}$$

$$\Phi_{\rm Ne}^B(\boldsymbol{R}_1,\boldsymbol{R}_2) = \sqrt{\frac{4!16!}{20!}}\mathscr{A}\{\psi_\alpha(\boldsymbol{R}_1,\boldsymbol{r}_1,\ldots,\boldsymbol{r}_4) \times \psi_{^{16}\rm O}(\boldsymbol{R}_2,\boldsymbol{r}_5,\ldots,\boldsymbol{r}_{20})\} \tag{7}$$

$$\propto \exp\left(-\frac{10(\boldsymbol{X}_G-\boldsymbol{R}_G)^2}{b^2}\right)\mathscr{A}\left[\exp\left(-\frac{8(\boldsymbol{r}-\boldsymbol{R})^2}{5b^2}\right) \times \phi(\alpha)\phi(^{16}\rm O)\right], \tag{8}$$

where $\boldsymbol{r}=\boldsymbol{X}_1-\boldsymbol{X}_2$, $\boldsymbol{R}=\boldsymbol{R}_1-\boldsymbol{R}_2$, $\boldsymbol{X}_G=(4\boldsymbol{X}_1+16\boldsymbol{X}_2)/20$, and $\boldsymbol{R}_G=(4\boldsymbol{R}_1+16\boldsymbol{R}_2)/20$. $\boldsymbol{X}_1$ and $\boldsymbol{X}_2$ represent the center-of-mass coordinates of the α cluster and ^{16}O cluster, respectively. $\Phi_{\rm Ne}^B(\boldsymbol{R}_1,\boldsymbol{R}_2)$ is the Brink cluster model wave function for ^{20}Ne. $\psi_\alpha(\boldsymbol{R}_1,\boldsymbol{r}_1,\ldots,\boldsymbol{r}_4)$ and $\psi_{^{16}\rm O}(\boldsymbol{R}_2,\boldsymbol{r}_5,\ldots,\boldsymbol{r}_{20})$ are the harmonic oscillator shell-model wave functions of the clusters α and ^{16}O located around $\boldsymbol{R}_1$ and $\boldsymbol{R}_2$, respectively. And $\phi(\alpha)$ and $\phi(^{16}\rm O)$ represent their intrinsic wave functions. For details, see Ref. [34]. It should be noted that we apply the same size parameter b in the $\alpha+^{16}$O system, for simplicity.

Furthermore, according to Eqs. (3) and (4), it is convenient to reduce the two parameters β_{1k} and β_{2k} to one parameter β_k by adopting the relations $1/(\beta_{1k})^2=1/(\beta_k)^2$ and $1/(\beta_{2k})^2=4/(\beta_k)^2$ $(k=x,y,z)$. Thus, the center-of-mass motion can be easily eliminated in the equation

$$\Phi_{\rm Ne}(\beta_x,\beta_y,\beta_z) = \int d^3R_1 d^3R_2 \exp\left\{-\left(\frac{R_{1x}^2}{\beta_x^2}+\frac{R_{1y}^2}{\beta_y^2}+\frac{R_{1z}^2}{\beta_z^2}\right)\right\} \times \exp\left\{-\left(\frac{4R_{2x}^2}{\beta_x^2}+\frac{4R_{2y}^2}{\beta_y^2}+\frac{4R_{2z}^2}{\beta_z^2}\right)\right\} \times \Phi_{\rm Ne}^B(\boldsymbol{R}_1,\boldsymbol{R}_2) \tag{9}$$

$$\propto \exp\left(-\sum_k^{x,y,z}\frac{10X_{Gk}^2}{B_k^2}\right)\mathscr{A}\left[\exp\left(-\sum_k^{x,y,z}\frac{8r_k^2}{5B_k^2}\right)\phi(\alpha)\phi(^{16}\rm O)\right], \tag{10}$$

where $B_k^2=b^2+2\beta_k^2$. One can easily grasp this merit from Eq. (10). When $\beta\to 0$, the intrinsic part of Eq. (10) corresponds to the SU(3) shell-model wave function of ^{20}Ne. When $\beta\to\infty$, Eq. (10) becomes $\phi(\alpha)\phi(^{16}\rm O)$, which corresponds to the state of two free clusters. Therefore, we believe that the wave function, Eq. (9), can describe the transient character of the ground-state band in ^{20}Ne.

In order to restore the symmetry of the system, we need to eliminate the center of total mass and make an angular momentum projection on the generalized THSR wave function, Eq. (9). For details, see Refs. [6] and [31].

To simplify the calculation of matrix elements, we transform $\boldsymbol{R}_1$ and $\boldsymbol{R}_2$ into the center-of-mass vector $\boldsymbol{R}_G$ and the relative vector $\boldsymbol{R}$:

$$\boldsymbol{R}_1 = \boldsymbol{R}_G + \tfrac{4}{5}\boldsymbol{R}, \tag{11}$$

$$\boldsymbol{R}_2 = \boldsymbol{R}_G - \tfrac{1}{5}\boldsymbol{R}. \tag{12}$$

All calculations are performed with restriction to axially symmetric deformation, that is, $\beta_x=\beta_y\neq\beta_z$. As for the two-cluster system, we can prove the following relation:

$$\frac{\langle\hat\Phi_{\rm Ne}^J(\beta_x,\beta_z)|\hat O|\hat\Phi_{\rm Ne}^J(\beta_x,\beta_z)\rangle}{\langle\hat\Phi_{\rm Ne}^J(\beta_x,\beta_z)|\hat\Phi_{\rm Ne}^J(\beta_x,\beta_z)\rangle} = \frac{\langle\Psi_{\rm Ne}^J(\beta_x,\beta_z)|\hat O|\Psi_{\rm Ne}^J(\beta_x,\beta_z)\rangle}{\langle\Psi_{\rm Ne}^J(\beta_x,\beta_z)|\Psi_{\rm Ne}^J(\beta_x,\beta_z)\rangle}. \tag{13}$$

Here, $\hat\Phi_{\rm Ne}^J(\beta_x,\beta_z)$ represents the internal spin-projected wave function of ^{20}Ne. $\Psi_{\rm Ne}(\beta_x,\beta_z)$ can be written as

$$\Psi_{\rm Ne}(\beta_x,\beta_z) = \int d^3R \exp\left\{-\left(\frac{4R_x^2}{5\beta_x^2}+\frac{4R_y^2}{5\beta_y^2}+\frac{4R_z^2}{5\beta_z^2}\right)\right\} \times \Phi_{\rm Ne}^B(\boldsymbol{R}). \tag{14}$$

The corresponding projected wave function is (see Ref. [6])

$$\Psi_{\rm Ne}^J(\beta_x,\beta_z) = \frac{2J+1}{8\pi^2}\times 4\pi^2\int d\cos\theta d_{00}^J(\theta) \times\int d^3R\exp\left\{-\left(\frac{4R_x^2}{5\beta_x^2}+\frac{4R_y^2}{5\beta_y^2}+\frac{4R_z^2}{5\beta_z^2}\right)\right\}\hat R_y(\theta)\Phi_{\rm Ne}^B(\boldsymbol{R}) \tag{15}$$

$$= \left(J+\frac{1}{2}\right)\int d\cos\theta d_{00}^J(\theta) \times\int d^3R\exp\left\{-\sum_k^{x,y,z}\frac{4}{5}\frac{(R_y(\theta)\boldsymbol{R})_k^2}{\beta_k^2}\right\}\Phi_{\rm Ne}^B(\boldsymbol{R}), \tag{16}$$

where $d_{00}^J(\theta)$ is the reduced Wigner d function. $\hat R_y(\theta)$ is the rotation operator representing the rotation by the angle θ around the y axis. $R_y(\theta)$ is the corresponding 3×3 rotation matrix. Because $\Phi_{\rm Ne}^B(\boldsymbol{R})$ can be written in the form of Eq. (8), Eq. (16) can be proved by using the relation $(R_y(\theta)\boldsymbol{r}-\boldsymbol{R})^2=(\boldsymbol{r}-R_y^{-1}(\theta)\boldsymbol{R})^2$. Thus, the final matrix element can be written as

$$\langle\hat\Psi_{\rm Ne}^J(\beta_x,\beta_z)|\hat O|\hat\Psi_{\rm Ne}^J(\beta_x,\beta_z)\rangle = \left(J+\frac{1}{2}\right)\int d\cos\theta d_{00}^J(\theta) \times\int d^3Rd^3R'\exp\left[-\sum_k^{x,y,z}\frac{4}{5}\frac{R_k^2+(R_y(\theta)\boldsymbol{R}')_k^2}{\beta_k^2}\right] \times\langle\Phi_{\rm Ne}^B(\boldsymbol{R})|\hat O|\Phi_{\rm Ne}^B(\boldsymbol{R}')\rangle. \tag{17}$$

In addition, for nondiagonal matrix elements, they also can be easily derived using the wave function, Eq. (16).

B. Microscopic Hamiltonian for ^{20}Ne

The microscopic Hamiltonian for ^{20}Ne in this work can be written as

$$H = T - T_G + V_N + V_C, \tag{18}$$

where T is the total kinetic energy operator and T_G the center-of-mass kinetic energy operator. The last two terms represent the effective two-body nuclear interaction and Coulomb interaction, respectively. These operators are given by the kinetic energy,

$$T = \sum_{i=1}^{20} \frac{-\hbar^2}{2m} \left(\frac{\partial}{\partial \boldsymbol{r}_i} \right)^2, \tag{19}$$

the center-of-mass kinetic energy,

$$T_G = \frac{-\hbar^2}{40m} \left(\frac{\partial}{\partial \boldsymbol{X}_G} \right)^2, \tag{20}$$

and the Coulomb potential,

$$V_C = \sum_{i>j}^{20} \frac{1-\tau_{zi}}{2} \frac{1-\tau_{zj}}{2} \frac{e^2}{\boldsymbol{r}_{ij}}. \tag{21}$$

The nuclear potential part is taken as Gaussian form. In this paper, the Volkov No. 1 Force [35] is adopted, which is expressed as

$$V_N = \sum_{i>j}^{20} \{(1-M) - M P_\sigma P_\tau\}_{ij} \sum_{n=1}^{2} v_n e^{-\frac{r_{ij}^2}{a_n^2}}. \tag{22}$$

C. Hill-Wheeler equation

Here, we give a brief outline of the GCM [36]. First, we construct the following wave function by superposing wave functions with good quantum numbers of angular momentum,

$$\Psi_k^J = \sum_\beta f_k^J(\beta) \hat{\Phi}_{\mathrm{Ne}}^J(\beta), \tag{23}$$

where $\beta \equiv (\beta_x, \beta_y, \beta_z)$. Ψ_k^J represents the kth normalized eigenfunction expanded in the basis of $\hat{\Phi}_{\mathrm{Ne}}^J(\beta)$. In order to determine the weight function $f_k^J(\beta)$, the following Hill-Wheeler equation should be solved:

$$\sum_{\beta'} \left\langle \hat{\Phi}_{\mathrm{Ne}}^J(\beta) \middle| \hat{H} - E \middle| \hat{\Phi}_{\mathrm{Ne}}^J(\beta') \right\rangle f_k^J(\beta') = 0. \tag{24}$$

We discretize the parameter β by adopting enough mesh points. Then the solution to the Hill-Wheeler equation is equivalent to the diagonalization of the Hamiltonian in the nonorthogonal basis of states $\hat{\Phi}_{\mathrm{Ne}}^J(\beta)$ [37].

III. RESULTS AND DISCUSSION

Without consideration of deformation, there are two parameters, b and β, in our wave function, and the minimum of the energy can be obtained by a full variational calculation with the two-parameter space. As for the nuclear interaction, the Volkov No. 1 Force [35] with a Majorana parameter $M = 0.6$ is adopted. In Fig. 1, we show the contour map of the energy surface of ^{20}Ne in the two-parameter space. The features of this map are similar to those of the corresponding maps of ^{8}Be, ^{12}C, and ^{16}O in previous papers [5,6]. The minimum energy appears at $\beta_x = \beta_y = \beta_z = 1.85$ fm and $b = 1.46$ fm, which can be considered a result of the competition of the size parameter of α particles and the size parameter of the whole nucleus. We fix the parameter $b = 1.46$ fm in our following calculations.

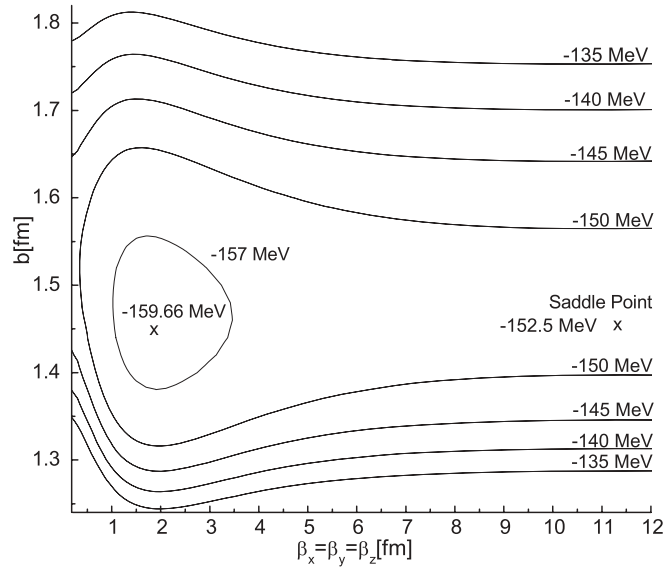

FIG. 1. Contour map of the energy surface of ^{20}Ne in the two-parameter space, b and $\beta_x = \beta_y = \beta_z$.

As we know, when $\beta \to +\infty$, ^{20}Ne can be regarded as a two-free-cluster structure so that there is almost no correlation between α and ^{16}O. That is, $E_{\mathrm{Ne}}(b, \beta \to +\infty) = E_\alpha(b) + E_{^{16}\mathrm{O}}(b)$. This simple relation makes it easy to obtain the minimum energy of a single ^{16}O particle by adopting the Volkov No. 1 Force with a Majorana parameter $M = 0.6$. Our calculations show that the binding energy of a single α particle takes its minimum value for the size parameter $b = 1.37$ fm, that is, $E_\alpha^{\min}(b = 1.37) = -27.08$ MeV. For the ^{16}O nucleus, the size parameter b becomes 1.49 fm with respect to the lowest energy of ^{16}O, namely, $E_{^{16}\mathrm{O}}^{\min}(b = 1.49) = -127.84$ MeV. This means that the calculated threshold energy is about 4.7 MeV, which is fully consistent with the experimental value 4.73 MeV. The asymptotic values of b parameters are slightly different from our adopted value $b = 1.46$ fm as is deduced appropriately from Fig. 1 for the more compact configurations of ^{20}Ne relevant here.

The valley has a saddle point at $\beta_x = \beta_y = \beta_z \approx 11.4$ fm and $b \approx 1.47$ fm. The height of the saddle point measured from the threshold energy is about 2.42 MeV and can be considered the Coulomb barrier. The state corresponding to the minimum energy can be considered approximately the ground state. The calculated result, -159.66 MeV, is in agreement with the experimental binding energy, -160.64 MeV, which suggests that the single generalized THSR wave function can

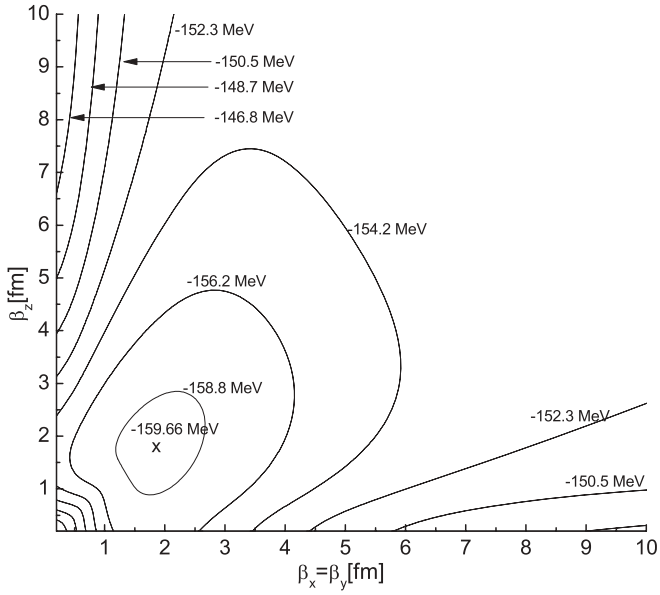

FIG. 2. Contour map of the energy surface of the deformed state of ^{20}Ne in the two-parameter space, $\beta_x = \beta_y$ and β_z.

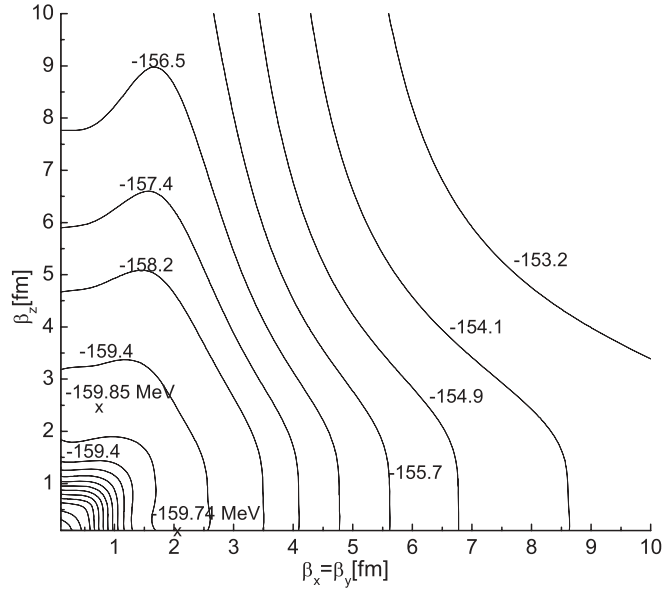

FIG. 3. Contour map of the energy surface of the $J^\pi = 0^+$ state in the two-parameter space, $\beta_x = \beta_y$ and β_z.

describe well the ground state of ^{20}Ne. This can be confirmed by comparison with the Brink cluster model in the following calculations.

Figure 2 shows the energy surface of the deformed state of ^{20}Ne in the two-parameter space, $\beta_x = \beta_y$ and β_z. The result indicates that the minimum energy lies on the $\beta_x(=\beta_y) = \beta_z$ line, which means that the minimum energy obtained, -159.66 MeV, corresponds to the spherical state. It should be pointed out that this result is obtained without angular momentum projection.

Next, we show the contour maps of the energy surfaces corresponding to different spin-projected states in ^{20}Ne in the two-parameter space, $\beta_x = \beta_y$ and β_z. They are calculated using the generalized THSR wave function without a single adjustable parameter, with the previously fixed parameter values. Figure 3 shows the contour map of the energy surface corresponding to the $J^\pi = 0^+$ state of ^{20}Ne after angular momentum projection in the two-parameter space, $\beta_x = \beta_y$ and β_z. It can be seen that the minimum energy no longer lies on the $\beta_x = \beta_z$ line but occurs at $\beta_x = \beta_y \approx 0.9$ fm and $\beta_z \approx 2.5$ fm in the prolate region of the map. The secondary minimum energy, -159.74 MeV, appears at $\beta_x = \beta_y \approx 2.1$ fm and $\beta_z \approx 0.0$ fm in the oblate region. There is a very narrow valley with a nearly flat bottom connecting the two minimum points, which indicates that the energy of the deformed configuration is slightly lower than that of the spherical configuration. The minimum energy, -159.85 MeV, indicates that the energy gain from the angular momentum projection is only about 0.19 MeV. Figure 4 displays the contour map of the squared overlap between the 0^+ wave function with $\beta_x = \beta_y = 0.9$ fm, $\beta_z = 2.5$ fm and the 0^+ wave function with variable $\beta_x(= \beta_y)$ and β_z. It can be seen that the oblate and prolate regions have very similar wave functions. In particular, the calculated squared overlap between the normalized wave function $\hat{\Phi}^{0^+}_I$, corresponding to the state of minimum energy, and $\hat{\Phi}^{0^+}_{II}$, corresponding to the state of secondary minimum energy, is about 0.999. This reveals that the two wave functions with respect to the minimum points are nearly equivalent. This conclusion is quite consistent with the description of ^{8}Be in the framework of the THSR wave function [6].

In Fig. 5 the energy surface of the $J^\pi = 2^+$ state is shown. We can see that there appears a maximum point at $\beta_x = \beta_y = \beta_z \approx 6$ fm with an energy of about -151 MeV. In fact, this energy region corresponds to the Coulomb barrier. As β decreases, we can also find a valley in the region confined by $\beta_x(\beta_y) + \beta_z - 2 > 0$ and $\beta_x(\beta_y) + \beta_z - 3.5 < 0$. It connects

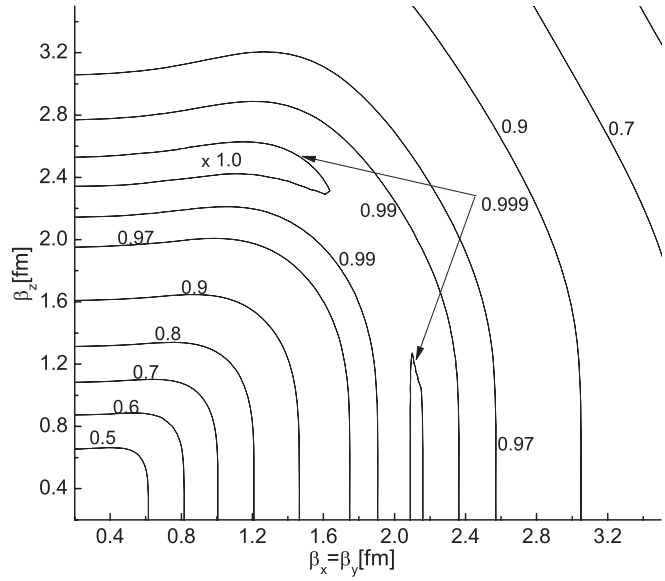

FIG. 4. Contour map of the squared overlap between the 0^+ wave function with $\beta_x = \beta_y = 0.9$ fm and $\beta_z = 2.5$ fm and the 0^+ wave function with variable $\beta_x(= \beta_y)$ and β_z. Numbers on the contour lines are squared overlap values.

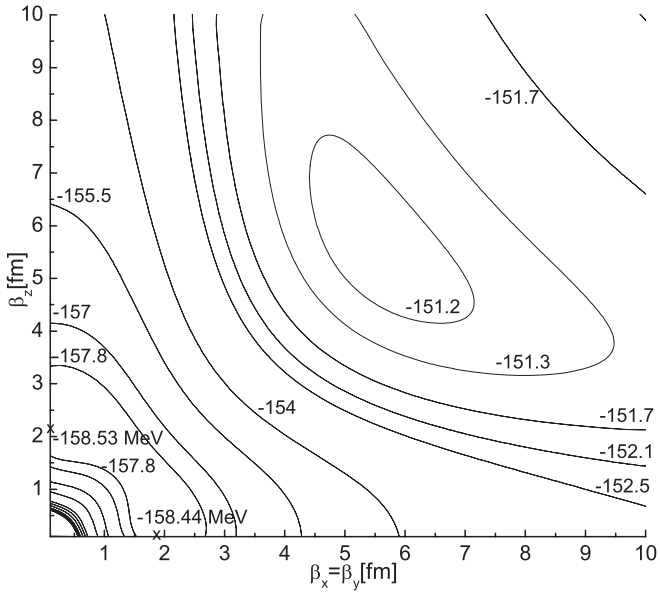

FIG. 5. Contour map of the energy surface of the $J^\pi = 2^+$ state of ^{20}Ne in the two-parameter space, $\beta_x = \beta_y$ and β_z.

the two minimum energy points. One is at $\beta_x = \beta_y \approx 0.0$ and $\beta_z \approx 2.2$ fm, with a minimum energy of -158.53 MeV in the prolate region of the plot. The other is at $\beta_x = \beta_y \approx 1.9$ fm and $\beta_z \approx 0.0$, with a secondary minimum energy, -158.44 MeV, in the oblate region. The two minimum energies are very close to each other. We can note that the energies do not change much in the valley, in spite of the fact that they correspond to completely different shapes. This can also be understood qualitatively by considering the squared overlap between the 2^+ wave function with $\beta_x = \beta_y \approx 0.0$ fm, $\beta_z \approx 2.2$ fm and the 2^+ wave function with variable $\beta_x (= \beta_y)$ and β_z. Figure 6

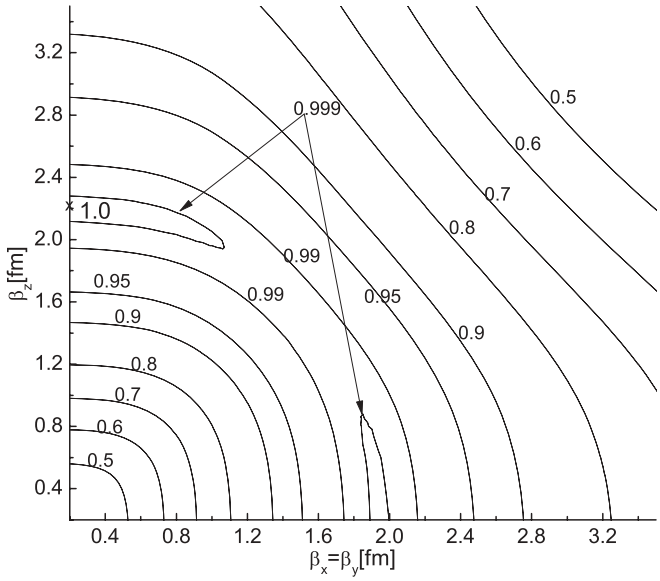

FIG. 6. Contour map of the squared overlap between the 2^+ wave function with $\beta_x = \beta_y \approx 0.0$ fm, $\beta_z = 2.2$ fm and the 2^+ wave function with variable $\beta_x (= \beta_y)$ and β_z. Numbers on the contour lines are squared overlap values.

shows again the similarity of the prolate and oblate states in the valley.

The contour map of the $J^\pi = 4^+$ state is very similar to Fig. 5. There also appears a maximum energy with respect to the top of the Coulomb barrier and a valley connecting the two minimum energies. The prolate and oblate regions correspond to similar wave functions according to our calculations.

As for the energy surfaces of the $J^\pi = 6^+$ and $J^\pi = 8^+$ states of ^{20}Ne, their binding energies become deeper as β_x or β_z becomes larger. That is, we cannot find a minimum of the energy in the two-parameter space, $\beta_x = \beta_y$ and β_z. This reflects the character of resonance states. However, one can obtain the local minimum energies in a small region. For the 8^+ state of ^{20}Ne, the two local minimum points both have an energy of -144.48 MeV. One is at $\beta_x = \beta_y \approx 0.0$ fm and $\beta_z \approx 0.7$ fm, and the other at $\beta_x = \beta_y \approx 0.7$ fm and $\beta_z \approx 0.0$ fm. The small β values indicate that the shell-model configuration prevails in this high-spin state.

As mentioned above, the oblate spin-projected intrinsic states are very similar to the prolate spin-projected intrinsic states from the energy contours of different states of the ground-state band in ^{20}Ne (see Figs. 4 and 6). This character can be explained by the structure of the spin-projected intrinsic wave function of ^{20}Ne [6]. Because the prolate and oblate deformed wave functions are approximately equivalent, we only superpose prolate deformed wave functions in GCM calculations. There is also a detailed discussion for ^{12}C in Ref. [9] about this situation. In order to solve the Hill-Wheeler equation, we adopt different mesh points of β_z by fixing β_x, which can avoid the numerical inaccuracy owing to the superposition of the similar wave functions and obtain a converged value. Our adopted mesh size of β_z is 0.5 fm.

In Table I, the (local) minimum energies and positions in the contour plots, the calculated energies of the ground-state band in ^{20}Ne, the GCM results, and the corresponding experimental values are listed. It can be seen that the GCM results and the calculated excited energies are in good agreement with the observed values, except for the energy of the $J^\pi = 8^+$ state. This proves the validity of our generalized THSR wave function for describing the compact cluster structure of ^{20}Ne.

Moreover, we can note that the parameter β_x or β_z, corresponding to the minimum energy or local minimum energy, becomes smaller as the spin increases from the energy contour plots, which is more clearly illustrated in Table I. Considering the meaning of the parameter β, we believe that the more cluster-model-like structure of ^{20}Ne is changing to a more shell-model-like structure as the spin J becomes larger. This is called the antistretching effect (e.g., see Ref. [38]), which is also discussed in the framework of the AMD [32]. Therefore, we conclude that the states of ^{20}Ne described by the $\alpha + ^{16}$O configuration gradually lose their collectivity as the spin increases and terminate in a shell configuration when $J^\pi = 8^+$. In fact, many calculations indicate that the termination of the ground-state band in ^{20}Ne appears at $J^\pi = 8^+$ [39]. In addition, the dominated shell configuration of $J^\pi = 8^+$ state might explain the larger error mentioned above. The reproduction of this antistretching effect within our model is very rewarding and demonstrates the flexibility of our wave function.

TABLE I. Minimum energies and corresponding distances between the α cluster and the ^{16}O cluster with respect to different spin-projected states in the Brink cluster model. The (local) minimum energies and their positions corresponding to the contour maps of energy surfaces of different spin-projected states, calculated excited energies of the ground-state band in ^{20}Ne, and observed values are listed. For low-lying states of ^{20}Ne, we list the GCM results obtained by the THSR model and the squared overlaps between our single normalized THSR wave function corresponding to the minimum energies and the normalized superposed Brink wave function, respectively. The squared overlaps between our single normalized THSR wave function and the single normalized Brink wave function corresponding to their (local) minimum energies are also listed. Units of energy are MeV.

State	$E^{\text{Brink}}_{\text{Min}}(R)$	$E^{\text{THSR}}_{\text{Min}}(\beta_x, \beta_z)$	Excited	$E^{\text{THSR}}_{\text{GCM}}$(excited)	Experiment	$\lvert\langle\hat{\Phi}^{\text{THSR}}_{\text{Min}}\rvert\hat{\Phi}^{\text{Brink}}_{\text{GCM}}\rangle\rvert^2$	$\lvert\langle\hat{\Phi}^{\text{THSR}}_{\text{Min}}\rvert\hat{\Phi}^{\text{Brink}}_{\text{Min}}\rangle\rvert^2$
0^+	−158.42(3.0)	−159.85(0.9, 2.5)	0	−160.05(0)	−160.64(0)	0.9929	0.9362
2^+	−157.19(2.9)	−158.53(0.0, 2.2)	1.33	−158.84(1.21)	−159.01(1.63)	0.9879	0.9494
4^+	−154.40(2.6)	−155.50(0.0, 1.8)	4.35	−156.04(4.01)	−156.39(4.25)	0.9775	0.9571
6^+	−150.18(2.1)	−150.80(0.0, 1.2)	9.05	–	−151.86(8.78)	–	0.9870
8^+	−144.30(1.5)	−144.48(0.0, 0.7)	15.37	–	−148.69(11.95)	–	0.9996

In order to further elucidate the generalized THSR wave function and obtain a deeper understanding of the cluster structure of ^{20}Ne, we make a comparison with the Brink wave function. The energy expectation $E_J(R)$ of the projected Brink wave function, which is a function of the intercluster distance parameter R, is expressed as

$$E_J(R) = \frac{\langle \Phi^{J^+}_{\text{Brink}}(R) | \hat{H} | \Phi^{J^+}_{\text{Brink}}(R) \rangle}{\langle \Phi^{J^+}_{\text{Brink}}(R) | \Phi^{J^+}_{\text{Brink}}(R) \rangle}. \tag{25}$$

The minimum energies and corresponding distances between the α cluster and the ^{16}O cluster with respect to different spin-projected states are calculated in the Brink cluster model. They are listed in Table I. For example, for the ground state of ^{20}Ne, when $R = 3.0$ fm, $E_0(R)$ takes its minimum value at −158.42 MeV. It should be noted that this energy is 1.43 MeV higher than the energy of −159.85 MeV obtained by our generalized THSR wave function. By adopting $R_j = 0.6 \times j$ fm, with $j = 1$–20, in the Hill-Wheeler equation, the GCM result −160.05 MeV is obtained. This result is consistent with the energy obtained by the THSR model in the GCM. Moreover, we compare our single generalized THSR wave function with the single Brink wave function and the superposed Brink wave function. The squared overlaps are listed in Table I.

For the $J^\pi = 0^+, 2^+, 4^+$ states of ^{20}Ne, it should be noted that the calculated GCM results within the Brink cluster model are basically in agreement with $E^{\text{THSR}}_{\text{GCM}}$(excited) in Table I. This indicates that the superposed THSR wave function and the superposed Brink wave function in the GCM are almost identical. By comparing the minimum energies of the Brink model and of the THSR model with the GCM energies for low-lying states of ^{20}Ne, we find that the minimum energies obtained by the single THSR wave function are much closer to the GCM energies.

Furthermore, it is found that the squared overlaps $|\langle\hat{\Phi}^{\text{THSR}}_{\text{Min}}|\hat{\Phi}^{\text{Brink}}_{\text{GCM}}\rangle|^2$ in Table I are very large. For the ground state of ^{20}Ne, the squared overlap, 0.9929, is nearly equal to 1. The large squared overlaps further indicate that our single generalized THSR wave function $\hat{\Phi}^{\text{THSR}}_{\text{Min}}$ is very close to the corresponding superposed Brink wave function $\hat{\Phi}^{\text{Brink}}_{\text{GCM}}$. On the other hand, the squared overlaps $|\langle\hat{\Phi}^{\text{THSR}}_{\text{Min}}|\hat{\Phi}^{\text{Brink}}_{\text{Min}}\rangle|^2$ are relatively small. For example, this value is only 0.9362 for the ground state of ^{20}Ne. This indicates that the single THSR wave function and single Brink wave function have some differences in describing low-lying states of the ground-state band in ^{20}Ne. Therefore, for describing the cluster character of low-lying states of the ground-state band in ^{20}Ne, the THSR model provides a more reasonable picture than the Brink cluster model.

For the more shell-model-like 6^+ and 8^+ states, it is found that the calculated (local) minimum energies are very close using the single generalized THSR and the single Brink wave function. In addition, the large squared overlaps, 0.9870 and 0.9996, further indicate that the single Brink wave function and the single THSR wave function are almost identical. These results can be well understood by the fact that the two kinds of wave function become the same SU(3) shell-model wave function at their shell limits ($\beta \to 0$ and $R \to 0$).

On the other hand, this comparison further proves that the more compact cluster structures of ^{20}Ne can be described well in the framework of the THSR model. In fact, we have described some non-gas-like structures in nuclei within the THSR model in the previous work. For instance, the normalized THSR state of ^{12}C gives the largest squared overlap, 0.93, with the ground state obtained by solving the Hill-Wheeler equation [20]. Considering that the ground state of ^{12}C contains no gas-like state but a more shell-model-like state with a large 3α correlation, the result indicates that it is very promising for treating non-gas-like cluster states in nuclei within the THSR model. Now, from the more cluster-model-like structure of the 0^+ state to the more shell-model-like structure of 6^+, the generalized THSR wave functions describe well these states of ^{20}Ne.

IV. SUMMARY

In this work, we have introduced a generalized THSR wave function for describing general cluster states in nuclei, which inherits the merits of the original THSR wave function characterized by a large spatial extension. As the first step, the ground-state band in ^{20}Ne is investigated within the microscopic cluster model.

First, the energies of the ground-state band in ^{20}Ne have been reproduced well with the generalized THSR wave function. Moreover, the antistretching effect of the ground-state

band is clearly shown, which provides a deeper insight into the transformation from the clustering to the shell-model-like states of the ground-state band in ^{20}Ne.

Furthermore, we make a comparison between our single generalized THSR wave function and the Brink wave function for the ground-state band in ^{20}Ne. It is found that our single generalized THSR wave function can reproduce accurately the low-lying states described by the GCM with the Brink wave function. We conclude that the THSR model provides a new picture for understanding the low-lying states of the ground-state band in ^{20}Ne. On the other hand, the successful description of the more compact cluster structure of ^{20}Ne provides strong support for our extension from the $n\alpha$ gas-like states to the general cluster states in nuclei.

It is worth mentioning that the other excited 0^+ states and important observables of ^{20}Ne such as the α-decay width can also be calculated in this generalized model. And the investigation of the ^{20}Ne is just the first step toward a generalized THSR wave function. More cluster structures in nuclei will be investigated in this framework. In addition, the negative-parity states being nontrivial, we will consider this problem and try to propose a way to deal with it using the spirit of the THSR model. These studies are in progress.

ACKNOWLEDGMENTS

This work was supported by the National Natural Science Foundation of China (Grant Nos. 10805026, 10975072, 11035001, 11120101005, and 11175085), by the 973 National Major State Basic Research and Development of China (Grant Nos. 2007CB815004 and 2010CB327803), by CAS Knowledge Innovation Project No. KJCX2-SW-N02, by Research Fund of Doctoral Point (RFDP) Grant No. 20100091110028, and by a project funded by the Priority Academic Program Development (PAPD) of Jiangsu Higher Education Institutions.

[1] K. Wildermuth and Y. C. Tang, *A Unified Theory of the Nucleus* (Vieweg, Braunschweig, 1977).
[2] K. Ikeda, H. Horiuchi, and S. Saito, Prog. Theor. Phys. Suppl. **68**, 1 (1980).
[3] M. Freer, Rep. Prog. Phys. **70**, 2149 (2007).
[4] W. von Oertzen, M. Freer, and Y. Kanada-En'yo, Phys. Rep. **432**, 43 (2006).
[5] A. Tohsaki, H. Horiuchi, P. Schuck, and G. Röpke, Phys. Rev. Lett. **87**, 192501 (2001).
[6] Y. Funaki, H. Horiuchi, A. Tohsaki, P. Schuck, and G. Röpke, Prog. Theor. Phys. **108**, 297 (2002).
[7] T. Yamada and P. Schuck, Phys. Rev. C **69**, 024309 (2004).
[8] T. Yamada and P. Schuck, Eur. Phys. J. A **26**, 185 (2005).
[9] Y. Funaki, A. Tohsaki, H. Horiuchi, P. Schuck, and G. Röpke, Eur. Phys. J. A **24**, 321 (2005).
[10] Y. Funaki, A. Tohsaki, H. Horiuchi, P. Schuck, and G. Röpke, Eur. Phys. J. A **28**, 259 (2006).
[11] P. Schuck, Y. Funaki, H. Horiuchi, G. Röpke, A. Tohsaki, and T. Yamada, Rom. Rep. Phys. **59**, 675 (2007).
[12] Y. Funaki, T. Yamada, H. Horiuchi, G. Röpke, P. Schuck, and A. Tohsaki, Phys. Rev. Lett. **101**, 082502 (2008).
[13] P. Schuck, Y. Funaki, T. Yamada, H. Horiuchi, G. Röpke, and A. Tohsaki, *AIP Conference Proceedings, Alpha-Particle Condensation in ^{16}O, Vol. 1165*, edited by M. Milin, T. Niksic, D. Vretenar, and S. Szilner (American Institute of Physics, Melville, NY, 2009), pp. 39–42.
[14] A. Tohsaki, H. Horiuchi, P. Schuck, and G. Röpke, Nucl. Phys. A **738**, 259 (2004).
[15] T. Yamada, Y. Funaki, H. Horiuchi, G. Röpke, P. Schuck, and A. Tohsaki, arXiv:1103.3940.
[16] Y. Funaki, A. Tohsaki, H. Horiuchi, P. Schuck, and G. Röpke, Phys. Rev. C **67**, 051306(R) (2003).
[17] Y. Funaki, A. Tohsaki, H. Horiuchi, P. Schuck, and G. Röpke, Mod. Phys. Lett. A **21**, 2331 (2006).
[18] Y. Funaki, T. Yamada, A. Tohsaki, H. Horiuchi, G. Röpke, and P. Schuck, Phys. Rev. C **82**, 024312 (2010).
[19] M. Itoh, H. Akimune, M. Fujiwara, U. Garg, N. Hashimoto, T. Kawabata, K. Kawase, S. Kishi, T. Murakami, K. Nakanishi, Y. Nakatsugawa, B. K. Nayak, S. Okumura, H. Sakaguchi, H. Takeda, S. Terashima, M. Uchida, Y. Yasuda, M. Yosoi, and J. Zenihiro, Phys. Rev. C **84**, 054308 (2011).
[20] Y. Funaki, H. Horiuchi, W. von Oertzen, G. Röpke, P. Schuck, A. Tohsaki, and T. Yamada, Phys. Rev. C **80**, 064326 (2009).
[21] A. Tohsaki, Int. J. Mod. Phys. E **17**, 2106 (2008).
[22] J. Hiura and F. Nemoto, and H. Bandō, Prog. Theor. Phys. Suppl. **52**, 173 (1972).
[23] Y. Fujiwara, H. Horiuchi, K. Ikeda, M. Kamimura, K. Katō, Y. Suzuki, and E. Uegaki, Prog. Theor. Phys. Suppl. **68**, 29 (1980).
[24] N. Itagaki, J. Cseh, and M. Płoszajczak, Phys. Rev. C **83**, 014302 (2011).
[25] M. Dufour, P. Descouvemont, and D. Baye, Phys. Rev. C **50**, 795 (1994).
[26] B. Buck, J. C. Johnston, A. C. Merchant, and S. M. Perez, Phys. Rev. C **52**, 1840 (1995).
[27] Y. Akiyama, A. Arima, and T. Sebe, Nucl. Phys. A **138**, 273 (1969).
[28] T. Inoue, T. Sebe, H. Hagiwara, and A. Arima, Nucl. Phys. **59**, 1 (1964).
[29] H. Horiuchi and K. Ikeda, Prog. Theor. Phys. **40**, 277 (1968).
[30] T. Matsuse, M. Kamimura, and Y. Fukushima, Prog. Theor. Phys. **53**, 706 (1975).
[31] H. Horiuchi and K. Ikeda, *Cluster Models and Other Topics, Vol. 4* (World Scientific, Singapore, 1986).
[32] Y. Kanada-En'yo and H. Horiuchi, Prog. Theor. Phys. **93**, 115 (1995).
[33] D. M. Brink, *Proceedings, International School of Physics "Enrico Fermi," Course 36* (Academic Press, New York, 1966).
[34] A. Tohsaki-Suzuki, Prog. Theor. Phys. Suppl. **62**, 191 (1977).
[35] A. B. Volkov, Nucl. Phys. **74**, 33 (1965).
[36] J. J. Griffin and J. A. Wheeler, Phys. Rev. **108**, 311 (1957).
[37] P. Ring and P. Schuck, *The Nuclear Many-Body Problem* (Springer-Verlag, New York, 2004).
[38] A. V. Afanasjev, D. B. Fossan, G. J. Lane, and I. Ragnarsson, Phys. Rep. **322**, 1 (1999).
[39] T. Une, Prog. Theor. Phys. **90**, 1269 (1993).